

PCCP

Accepted Manuscript



This is an *Accepted Manuscript*, which has been through the Royal Society of Chemistry peer review process and has been accepted for publication.

Accepted Manuscripts are published online shortly after acceptance, before technical editing, formatting and proof reading. Using this free service, authors can make their results available to the community, in citable form, before we publish the edited article. We will replace this *Accepted Manuscript* with the edited and formatted *Advance Article* as soon as it is available.

You can find more information about *Accepted Manuscripts* in the [Information for Authors](#).

Please note that technical editing may introduce minor changes to the text and/or graphics, which may alter content. The journal's standard [Terms & Conditions](#) and the [Ethical guidelines](#) still apply. In no event shall the Royal Society of Chemistry be held responsible for any errors or omissions in this *Accepted Manuscript* or any consequences arising from the use of any information it contains.

ARTICLE

Multiscale approach for studying melting transitions in CuPt nanoparticles

Cite this: DOI: 10.1039/x0xx00000x

Luca Pavan^a, Francesca Baletto^a and Rada Novakovic^b

Received 00th January 2012,
Accepted 00th January 2012

DOI: 10.1039/x0xx00000x

www.rsc.org/

A multiscale approach, based on the combination of CALPHAD and molecular dynamics (MD) simulation, is applied in order to understand the melting transition taking place in CuPt nanoalloys. We found that in systems containing up to 1000 atoms, the morphology adopted by the nanoparticles causes the icosahedral CuPt to melt at temperatures 100 K below that of the other morphologies, if the chemical composition contains less than 30% of Pt. We show that the solid-to-liquid transition in CuPt nanoparticles of a radius equal to or greater than 3 nm could be studied using classical tools.

1 Introduction

There has been increasing interest in multi-metallic systems, due to their peculiar physical and chemical properties that could be used in a wide range of applications, such as magnetism, plasmonics, electrochemistry and environmental engineering, and biomedicine.¹⁻² Breaking the bulk translation symmetry of a metallic system may lead to the presence of new physical properties, with respect to their bulk counterpart. For this reason, the combination of two metals offers an almost endless flexibility in terms of property tuneable as a function of system size, chemical composition, and chemical ordering compared with their elemental counterparts. In general, bimetallic nanoalloys form a core-shell, fully segregated Janus, random or ordered alloyed patterns, and evaluating their phase diagrams is a very active field of research.³⁻⁹ Nonetheless, there is always an interest in understanding the stability/instability of a chemical pattern, and/or of a specific structural motif adopted. In specific, the dependence of the melting/freezing transition on the size and shape of the nanoalloys is still an unsolved puzzle.^{10,11}

The limited amount of Pt, together with its high cost, requires the development of new alloys with comparable catalytic activity and a reduced Pt-content.^{12,13} The bulk Cu-Pt system has been investigated as an alternative to pure Pt and Pt-group catalysts or as a subsystem of Cu-Pt-Zr, Cu-rich glassy alloys containing a small amount of Pt, used for highly active methanol steam reforming catalysts.¹⁴ It has been shown that the unique properties of nanosized metals and alloys can offer solutions to engineering problems that are not possible using conventional alloyed metals.

Pt-based nanoparticles are found to show a higher reactivity than those consisting of pure platinum, especially for the conversion of CO₂, and as electrocatalysts in fuel cells for oxygen reduction.¹⁵⁻¹⁸ It is important to mention that coalescence has a detrimental effect on catalysis, due to a reduction in the electrochemically active surface area that reduces cell performance. However, in some applications, such as the fabrication of thick film conductors, the ability to enhance coalescence and the sintering processes is beneficial in order to produce high conductivity lines at low temperatures, and allow the development of many novel devices.¹⁹ Accordingly, knowledge of the favourable operative conditions for the coalescence of metallic nanoparticles at a multi-scale level are a necessary prerequisite for many applications. Very recently, several experimental groups have worked on the synthesis of CuPt. This compound exhibits a wide range of chemical patterns, i.e. core-shell, onion-like and alloyed, within various morphologies, such as cubes and spheres.²⁰⁻²³ CuPt nanoparticles can be exploited as nanocatalysts thanks to their excellent catalytic activities, for CO and ethanol oxidation, as well as for the oxygen reduction.²⁴ Although the importance and potential use of CuPt nanoparticles have been examined, few studies addressed their stability with regards external factors, such as temperature. The large surface area in nanosized systems results in high reactivity and many interactions between intermixed materials, leading to specific properties, such as melting temperature depression.²⁵

Here we study the melting/freezing transition of large, 3-6 nm radius, CuPt nanoparticles using a multiscale approach. A “top-bottom” methodology, based on thermodynamic models, is used to study the melting temperature depression as a function of nanoparticle radius. At the same time, an atomistic “bottom-up” approach based on molecular dynamics simulations is

applied, in order to address the issue of whether the shape and the chemical ordering has any effect on the system.

The manuscript is divided as follows: we describe both numerical approaches, then we show our predictions within the framework of classical theory, and then we discuss our atomistic simulation results.

2 Thermodynamic models and atomistic approaches

Our methodology is a combination of “top-down” (thermodynamic and CALPHAD method) and “bottom-up” (atomistic molecular dynamics) approaches. Phenomenological considerations led Thompson²⁶ and Pawlow²⁷ to develop independently quantitative relationships between the melting temperature of a small particle and its size, showing that the melting temperature depression increases with a decrease in particle size. Based on their idea, many different theoretical models have been developed in order to predict the depression of the melting point with respect to the bulk value, as a function of the radius of the nanoparticle, which is assumed to be spherical. The thermodynamic models, recently reviewed by Barybin and Shapovalov in describing the melting behaviour of nanosized particles have been experimentally verified on pure metals, confirming that the melting temperature depression and particle size are inversely proportional, at least in a size range above several nm. In the following, the melting behaviour of Cu and Pt nanoparticles has been predicted within the liquid layer model (LLM) model,²⁹ as this exhibits the best agreement with the experimental data on Cu,³⁰ while in the case of Pt,³¹ a scatter observed was significantly lower in comparison to the results obtained by the other models listed in.²⁸ In the LLM, the melting temperature depression is given by

$$\frac{\Delta T_m(r)}{T_m^{\text{bulk}}} = \frac{v_s 2\sigma_{sl}}{\Delta H_m r} \left[1 + \frac{r}{r+l} \frac{\sigma_l}{\sigma_{sl}} \left(1 - \frac{v_l}{v_s} \right) \right] \quad (1)$$

where ΔH_m^{bulk} and T_m^{bulk} are the molar heat of fusion and melting temperature of the bulk; v_s and v_l are the molar volume of the solid and liquid, respectively. σ_s , σ_l and σ_{sl} are the interfacial energies of the solid-gas, liquid-gas and solid-liquid, respectively, while r and l are the nanoparticle radius and critical thickness of the liquid layer.

The phase diagram and hence the melting behaviour of bimetallic nanoalloys can be calculated by the Calphad (“Calculation of Phase Diagrams”) method,³² that has been widely used for the study of phase equilibria of binary, ternary and multicomponent systems as well as for the calculations of their phase diagrams. In order to calculate the phase diagrams of nano-sized alloys, Tanaka and Hara extended the Calphad method taking into account the effect of surface energy on the thermodynamic properties of small systems,³³ where a minimization of the total Gibbs free energy of a small system gives its phase diagram as a function of particle size. The molar Gibbs energy of the entire system is given by the sum of the molar Gibbs energies of the phases present in the system. The surface energy term containing the surface tension, molar volume,

correction factor and particle radius is added to the Gibbs free energy of each phase of the system. The surface tension of a binary liquid alloy phase can be calculated from the Butler equation where the partial surface excess Gibbs energy is related to the bulk one throughout a parameter corresponding to the ratio of the coordination numbers in the surface phase to that in the bulk, as we discussed in our previous work.³⁴ It has been shown that the Calphad method is appropriate for simple binary nanosized systems, characterised by lens type phase diagrams, such as AuAg³⁵ and CuNi,³⁸ or eutectic, as AgCu,³⁶ and peritectic alloy systems,³³ while for compounds forming nanosized systems due to complex phase equilibria, its application requires some simplifications.³⁹ The lower size limit used when applying the Calphad method for nanosized binary alloy systems and subsequently their phase diagram is system dependent, but generally the smallest particle radius is estimated to be 4-5 nm.^{28,37}

Our “bottom-up” approach consists in the modelling of the melting/freezing phase transition over a wide cluster size range, using a classical molecular dynamics (cMD) tool. A velocity-Verlet algorithm is applied in order to integrate Newton’s equations of motion with a time step of 5 fs. The temperature of the whole system is varied at a constant rate, referred to as the melting/freezing rate. An Andersen thermostat, with a frequency set in such a way that the diffusion properties of the system are not affected, controls the temperature between two subsequent increments. In our previous work,⁴¹ we have shown that this approach can be successfully applied to nanoalloys showing that few impurities could change dramatically the melting temperature of sub-nanometre clusters. Furthermore, we have performed few growth simulations in order to understand the preferential chemical ordering in CuPt. The growth model is the one described in our previous works,^{3,42} where atoms were deposited one-by-one over an existing core. Between two subsequent depositions, all the atoms of the clusters are free to move, and the temperature is kept constant throughout an Andersen thermostat. Our growth simulation results are summarised in Section 3.3. In any event, the interparticle potential assumes the analytic form proposed by Rosato-Guillopo-Legrand (RGL), a second-moment approximation of the tight binding method, in which the atomic contribution to the total energy is

$$E_i = \sum_{j \neq i} A_{\alpha\beta} \exp \left[-p_{\alpha\beta} \left(\frac{r_{ij}}{r_{\alpha\beta}^0} - 1 \right) \right] - \sum_{j \neq i} \xi_{\alpha\beta}^2 \exp \left[-2q_{\alpha\beta} \left(\frac{r_{ij}}{r_{\alpha\beta}^0} - 1 \right) \right], \quad (2)$$

where the repulsive potential has a Born-Mayer form.

In Eq.(2), r_{ij} is the interatomic distance between each pair, while the nearest-neighbour distance is labelled with $r_{\alpha\beta}^0$. The label “ $\alpha\beta$ ” refers to the different chemical species. For a homoatomic pair, $r_{\alpha\alpha}^0$ and $r_{\beta\beta}^0$ coincide with their bulk nearest-neighbour distances, while for hetero-type pairs this is given by

the arithmetical average of the two homo-atomic values. For homo-atomic interactions, the four parameters, A , ξ , p and q , appearing in Eq. 2, are fitted in order to reproduce the experimental values of the cohesive energy, lattice and elastic constants (such as bulk modulus). ξ is related to the attractive energy, A to the repulsive energy, p and q are ranges of interactions and their product determines the width of the potential well. The numerical value is taken from Ref. [43]. The mixed parameters are instead obtained by averaging the pure ones. This appears to reproduce the general trend of having a Cu-shell, and even an onion-shell ordering, as predicted recently using grand-canonical Monte-Carlo with an *ad-hoc* embedded-atom model.²³

3 Results

First of all, we would like to discuss our cluster size range choice. It has been recently shown that the thermodynamics arguments might be extrapolated for particles with a radius of 2-4 nm. At smaller sizes, the phonon diffusion length is of the same order of the maximum pair distance and it is a challenge to define the cluster temperature.⁴⁴ It has been demonstrated that a thermodynamic theory is valid for PdPt nanoparticles of 4 nm.¹¹ The same authors have further addressed the shape effect for gold, silver, and nickel clusters.¹⁰ From those studies, it appears that the shape factor is quite significant comparing cube, tetrahedron, sphere and icosahedra, but less important if one compares icosahedron, truncated octahedron respecting the Wulff construction.⁴⁵ Saying that, we are expecting that the shape factor clearly plays a role for systems containing up to 1000 atoms, but it is likely to be less and less important at larger sizes. In addition, our growth simulations in the sub-nano regime, show that the main geometrical motifs for CuPt are the decahedron (Dh) and FCC shapes, reminiscent of a Wulff truncated octahedron (TO) or of a cubo-octahedron (Co) with several stacking faults. The Co belongs to the truncated-octahedron family delimited by triangular (111) facets alternating square (100) facets, while the Wulff-TO, or simply TO, shows regular hexagonal (111) and square (100) faces.

3.1 Thermodynamic prediction of the melting transition of nanosized systems

The calculation of the phase diagram of Cu-Pt nanoalloys has been done taking into account the descriptions of new phases using the Gibbs free energy data⁴⁶ and the surface energy terms expressed by the surface tension of the liquid^{47,48} or solid phases⁴⁹ together with the molar volumes of the liquid⁵⁰ or solid phases.⁵¹ For the sake of clarity, the values used are summarized in Table 1.

Table 1 The parameters used for the calculations of the melting temperature of Cu, Pt and CuPt nanoparticles

	Cu	Pt	CuPt
T_m (K)	1356.15 ⁵⁰	2047.15 ⁵⁰	≈ 1844 ⁴⁶
T_b (K)	2903.15 ⁵⁰	4077.15 ⁵⁰	
σ_l (Nm ⁻¹)	1.367 ⁴⁷	1.800 ⁴⁸	1500 ^{calc.}
σ_s (Nm ⁻¹)	1.592 ⁴⁹	2.482 ⁴⁹	
σ_b (Nm ⁻¹)	0.234 ²⁸	0.271 ^{calc.}	
v_s (cm ³ mol ⁻¹)	$7.580 \cdot 10^{-6}$ ²⁸	$9.020 \cdot 10^{-6}$ ⁴⁷	
v_l (cm ³ mol ⁻¹)	$8.000 \cdot 10^{-6}$ ²⁸	$10.310 \cdot 10^{-6}$ ⁵⁰	
l (nm)	1.000 ^{estim.}	1.000 ^{estim.}	
G_{Cu-Pt}^{ss} (J mol ⁻¹)			Optimized data sets ⁴⁶

After optimization, due to uncertainties in the data of thermo-physical properties, the results obtained seemed to be correct for particle radii greater than 25 nm. Because of that, the results obtained by the Calphad method have been compared to the “liquidus and solidus curves” calculations, in the simplified version for lens type phase diagrams described in Ref. [48]. Using that method, we have calculated a difference up to 72 K, while in the bulk phase diagram it is 60 K, between the liquidus and solidus temperatures. Combining the LLM in Calphad and the corrections provided by the calculus of liquidus and solidus curve, we have calculated the melting temperature of CuPt

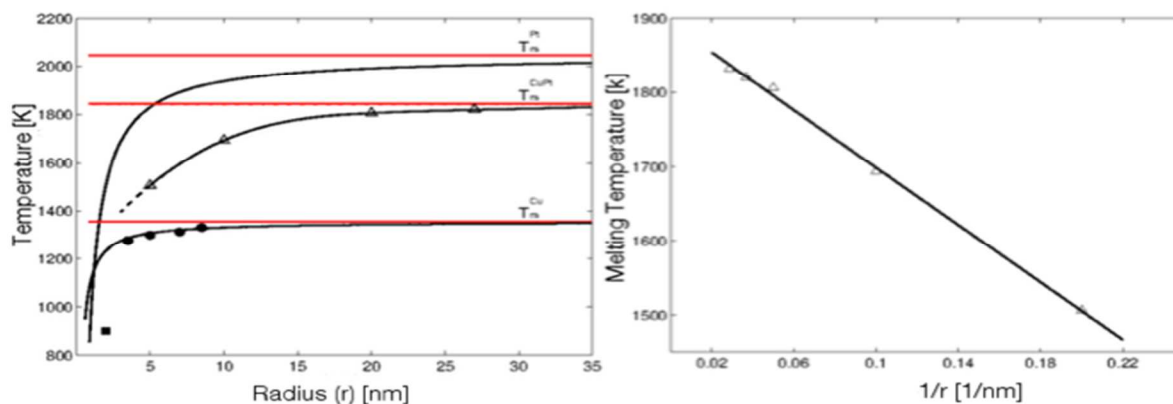


Fig. 1 Left panel: Calphad thermodynamic prediction of the melting temperature depression of elemental Cu, Pt (Eq. 1) and bimetallic CuPt nanoalloys at 1:1 composition. Red lines refer to the bulk melting limit for pure metals and its alloy. The full symbols correspond to the experimental data for Cu and Pt taken from Refs.[30,31] while the open triangles refer to the calculated points by the Calphad method. Right panel: The linear dependence of the melting transition versus $1/r$ is shown for CuPt.

nanoparticles with a radius varying between 3 and 40 nm. Our results for the pure metals and the 1:1 chemical composition are shown in Fig. 1. The melting temperature depression of a 3 nm cluster has been estimated in order to have a direct comparison with the atomistic approach discussed later. In the left panel of Fig. 1, the bulk reference values have been added. Furthermore, we have analysed our thermodynamic prediction fitting the relationship $\Delta T_m \propto r^{-1}$, as shown in the right panel of Fig. 1. As expected since the works of Thompson and Pawlow,^{26,27} a linear dependence of the melting temperature, and hence of the melting depression has been verified, as in the case of BiPb nanoparticles.³⁷ The fitted line is $T_m = -1482.3*(1/r) + 1859.2$, being r the radius of the nanoparticle.

3.2 Melting and Freezing throughout atomistic simulations

For a direct comparison with the Calphad results, we focused our attention on large systems and using a reasonably low rate. Three nanoparticle sizes of 309, 923 and 6266 atoms, corresponding to a diameter of 1.8 nm, 3.3 nm and 6 nm, respectively, have been selected. For the 309 and 923 atoms systems, a melting/freezing rate of 50 K/ns, and the cluster temperature, T , was varied between 800 and 1600 K. The 6266 atoms clusters were heated at rates of 50, 100 and 500K/ns between 1000 and 1600 K and then cooled at a rate of 40 K/ns. Our results have been averaged over at least five separate simulations. The melting temperature has been defined as the average between the temperatures at which a phase transition happens during a melting and a freezing. This corresponds to the peak in the specific heat.

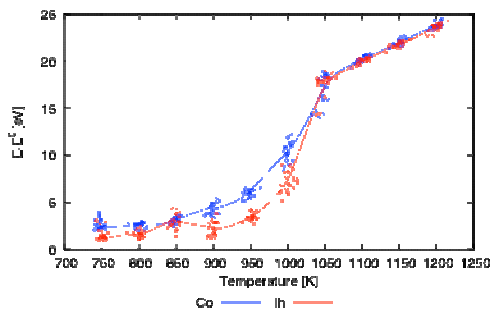


Fig. 2 Caloric curves of Co (blue) and Ih (red) at 309 atoms, for a CuPt 1:1 composition. The potential energy, in eV, is rescaled against its value E_0 of the structure at 0 Kelvin. The Ih undergoes to a structural change around 800 K.

At 309 atoms, we have considered a cubo-octahedron (Co) and an icosahedron (Ih) for a 1:1 chemical composition with a Cu-shell@Pt-core, or a randomly alloyed chemical order. Although a mixing is expected in the bulk limit, our growth simulations show that a Cu-rich uppermost shell is likely to form. Our results are summarised in Fig. 2 where the caloric curves are plotted. The caloric curve is the potential energy rescaled with respect to the value of the corresponding shape at 0 Kelvin, as a function of the averaged temperature. The melting occurs at 1050 +/- 50 K independently of the chemical ordering chosen at

the beginning. Thus, we show our analysis for the core-shell case. Our structural 'on-the-fly' analysis involves the monitoring the number of homo and hetero bonds and the mapping of the chemical ordering throughout a radial chemical distribution function (RCDF), reported in Fig. 3. The RCDF is defined as the molar ratio of Pt in the volume delimited by two spherical surfaces centred on the centre of the whole nanoparticle and having radii r and $r+\varepsilon$, for r that takes all the values integer multiples of ε from zero to the maximum pair distance of the cluster. The thickness, ε , is kept fixed at 0.3 Angstrom. The colour of each dot signifies the chemical composition, from rich (blue) to poor (red) in Pt. The number of homo- and mixed bonds reveals a chemical rearrangement in which Cu is diffusing towards the centre of the clusters and a mixed interlayer is formed. This migration is more evident in the case of Ih than in the case of Co. In any event, before the melting, the formation of an onion-like structure with a Cu-

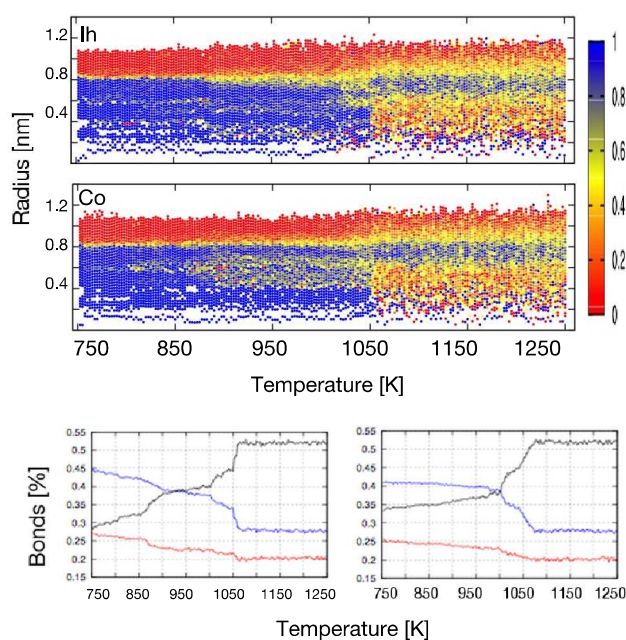


Fig. 3 RCDF and number of bonds during the melting of a Ih and a Co CuPt clusters at 1:1 chemical composition.

shell, a mixed sub-shell and a Pt-core is observed. After the melting, the liquid shell is still rich in copper, but its thickness is reduced and many copper atoms diffuse towards the centre.

At 923 atoms, we have considered the Ih, Co and the Dh at five different compositions, corresponding to a copper molar concentration of 0, 0.25, 0.50, 0.75, and 1. A mixed and random chemical ordered has been chosen. Thanks to the analysis of the melting of the three structural motifs we should be able to address if there is any shape effect that could be added eventually into the classical analysis. The caloric curves obtained for the 923-atoms cases are reported in Fig. 4.

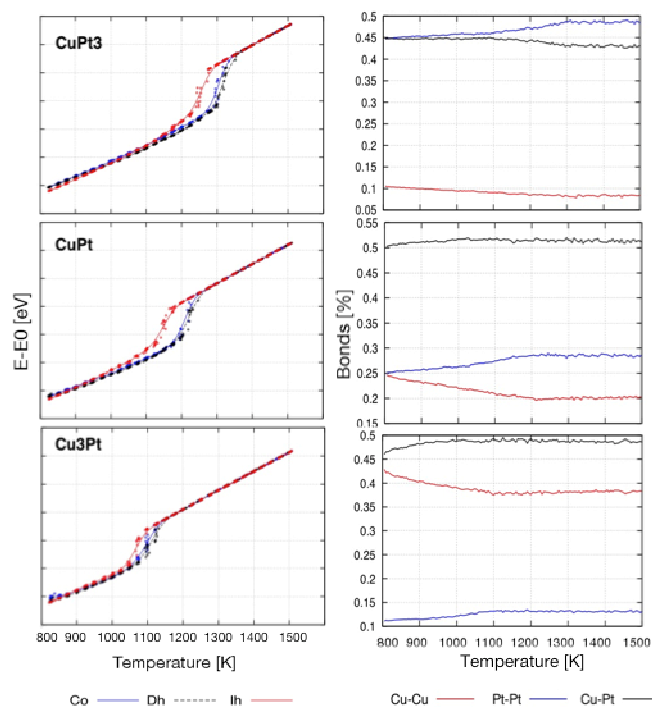


Fig. 4 Caloric curves, for the 923 atoms cubo-octahedron (blue), decahedron (black) and icosahedron (red). The Pt concentration grows from bottom to upper panel. On the right column, the evolution during the melting of the number of homo and hetero bonds (in %) in a Co per each molar composition. Similar results have been obtained for Ih and Dh.

The shape effect is still present in fact the Ih melts at a lower temperature than the Dh and the Co, except for very Cu-rich clusters. Fig. 5 summarises how the melting temperature changes varying the Pt-concentration. A linear behaviour is observed for all structural motifs, as expected as the number of mixed CuPt pairs is between 40-50% in all the considered cases. It should be noted that Co and Dh show an increase of the T_m of 5.12 K/Pt-concentration while the slope lowers to 4.3 K/Pt-concentration for Ih. This difference is related to the fact that platinum dislikes the icosahedral motif, while Cu-Ih is still energetically favourable.

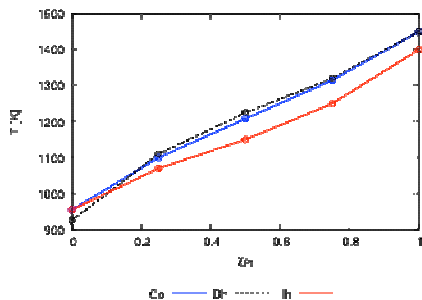


Fig. 5 Melting temperature, in Kelvin, dependence on the molar Pt-concentration.

Regarding the chemical ordering, there is clear tendency to form a Cu-shell, a mixed subsurface layer and then a third region Pt-rich, although we were starting from a randomly

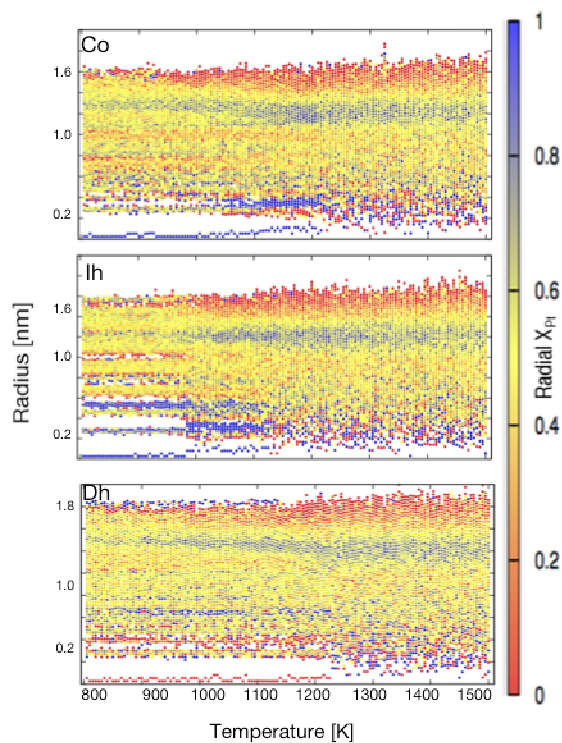


Fig. 6 Time evolution of the RCDF for a cubo-octahedron (top), decahedron (bottom), icosahedral (middle) at 923 atoms and equi-composition. The colours scheme refers to the molar density where blue and red mean high and low Pt %, respectively.

mixed case, as depicted in the RCDF shown in Fig. 6. The inner core is usually Pt-rich, except for the Dh where potentially a four-onion shells chemical pattern is found at least up to 50% of Pt, where we found mainly Cu in the inner, followed by a Pt-rich and then a mixed layer, and the outermost layer is still Cu-rich. The melting transition corresponds when the core starts to be disordered. We should note that, especially for the cubo-octahedron, just before the melting there is the formation of a Pt-rich layer. Furthermore, even at very high T, as high as 1600 K, where the cluster is melted independently of its chemical composition, we have that Cu atoms still decorate the surface of the liquid droplet. For quantifying the mixing, the number of homo-pair and the hetero-pairs has been monitored during the melting simulation. It turns out that the number of mixed pair is roughly constant for all the chemical composition, with just a small increase or decrease close to the melting transition, as reported in Fig. 4. The number of Cu-Cu bond (red line in the right panel of Fig. 4) decreases at the melting point independently of the chemical composition chosen. This should be explained in terms of the fast diffusion of copper towards the low coordinate sites at the surface. On the other hand, Pt atoms still occupy inner position and thus the number of pure Pt-Pt pair should eventually increase when the melting takes place.

For the largest system, a TO of 6266 atoms, we have considered only a randomly mixed chemical ordering. The melting/freezing transition of this 6 nm, alloyed nanoparticle is depicted in Fig. 7, where the caloric curve is plotted.

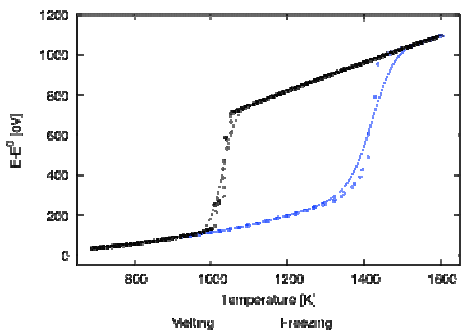


Fig. 7 Caloric curve during the melting/freezing of a truncated octahedron of 6266 atoms CuPt with mixed chemical pattern.

First of all, we would like to comment the huge hysteresis that takes place –the freezing temperature is about 400 K less than the melting point–, where apparently a super cooled liquid droplet is formed with a Cu-rich shell, then a strongly mixed subshell, a third Pt-rich layer, as depicted in the RCDF as reported in Fig. 8. Let us first discuss the freezing.

One should note that the solidification happens in two stages: the first one when the radius of the cluster shrinks and there is the formation of few solids small regions ($T_1 \sim 1400$ K) but the region around the centre of mass is still not formed, and the second stage, when an ordered inner core starts to be formed

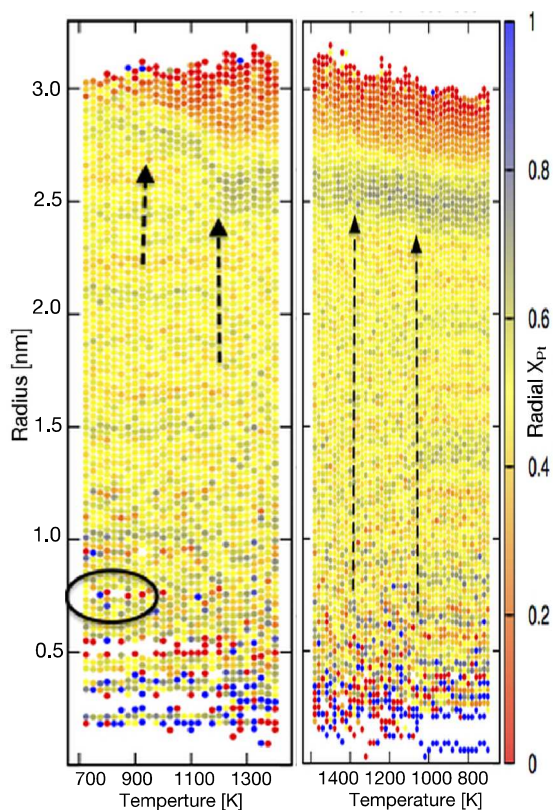


Fig. 8 Time evolution of the RCDF for a TO of 6266 atoms for melting (left) and freezing (right). Black arrows indicate the two stages during the solid-to-liquid –and vice versa– transition. Blue dots refer to a Pt-rich region, while red are for a Cu-rich one.

($T_2 \sim 1025$ K). Furthermore, one should note that the droplet solidifies in a centred structure –meaning that there is a Pt atom very close to the geometrical centre of mass. From the caloric

curve one can identify the freezing when the ordering of the inner shells takes place.

In the data obtained from the melting simulations, we observed a stage in which Cu atoms are quite mobile (T between 1100–1300 K), and the cluster is slightly expanding. Eventually the diffusion is helped by a kind of vacancies, highlighted in Fig 8, not corresponding to geometrical shells. In that wide temperature range, the structure is still well defined and we observed a quite significant increase of copper atoms at the surface. At the same time, we can easily notice the formation of an alloyed sub-surface layer and a Pt-rich region as third shell. As the temperature increases, the RCDF shows a broadening of the platinum region shell.

3.3 Growth atomistic simulations

Few growth simulations at 600 K have been carried out starting from different cores between 55 and 75 atoms, and then depositing Cu or Pt atoms one-by-one to 200 atoms, following. The deposition rate was of one atom each ns. The deposition is in such a way that Cu or Pt atoms are deposited with the same probability and in order to keep roughly a 50% of the chemical composition. The starting cores were a copper icosahedron or cubo-octahedron of 55 atoms or a decahedron core at 75 atoms. The structural evolution shows that after few depositions, the Ih is not any longer favoured but face-centre-cubic or decahedral geometry is formed. Often the decahedron has its 5-fold axis very close to the surface, in such a way that the formation of face-centre-cubic motifs with several stacking fault planes is very likely. In terms of the chemical ordering we observe that a good intermixing occurs although a Cu-rich surface has been formed while Pt seems to prefer to occupy core sites. Cu atoms are more mobile than the platinum ones, as one should expect as Pt is more cohesive than copper. When the decahedron is the initial configuration this is maintained and it is likely to have a copper-shell upon a Pt core. The presence of Cu at the surface should be due to its favourable surface energy with respect to platinum. A platinum core should also explain why the icosahedral shape is not favoured even at such small sizes, as Pt usually prefers the decahedral motifs at these size ranges.⁴¹

4 Discussion and Conclusions

A combination of thermodynamic and atomistic simulations has been applied in order to study the depression of melting points in CuPt nanoalloys. We find that for CuPt clusters of a radius between 1.5 and 3 nm, melting occurs between 950 and 1500 K, depending on the Pt concentration, where platinum-richer clusters exhibit a higher melting temperature. For clusters with a radius up to 1.6–2 nm, there is still a shape effect, as the melting transition of decahedra and truncated octahedrons melt at slightly higher temperatures than Ih. Nonetheless, this effect is small, and this is in agreement with the predictions made for similarly shaped PtPd nanoparticles with a radius of 4 nm.^{8,9,53} We would like to stress that if a structure is very unfavourable for a given chemical composition, it will rearrange toward a more stable shape before melting. We have found that the thermodynamic approach gives important and useful insights into the thermal behaviour of nanoparticles with a radius above 3–4 nm. Below a radius of 3 nm, the shape effect eventually is important and classical thermodynamic models appear to greatly underestimate the melting temperature, as depicted by our linear extrapolation in Fig. 9, against the estimates obtained

using a molecular dynamics approach. The 3–4 nm size range seems to be a promising size range where the classical and the atomistic simulations might be combined. To improving the agreement between these models and experimental data, other physical factors such as interatomic diffusion, and then a change of the chemical compositions in each layer, and the

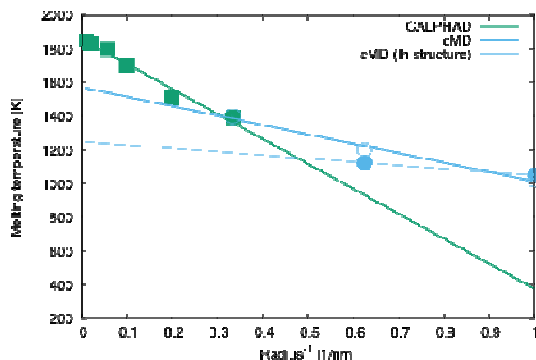


Fig. 9 Comparison between the thermodynamic and atomistic models adopted in this work. Each atomistic point is affected by an error of ± 50 K. The lines have been obtained by the least squares fitting.

dependence of the surface tension by the chemical ordering, should be explicitly taken into account. Nonetheless, the comparison of dynamic and thermodynamic models for a 3 nm nanoparticle reveals a supercooled region. As Calphad and cMD predict similar melting temperature, within a few degrees, the huge melting/freezing hysteresis of the TO at 6266 atoms could be explained in terms of the formation of a supercooled phase. This effect should be confirmed by experimental evidence and we hope that our work will stimulate further research in this direction. At the same time, it would be of great importance to develop a thermodynamic model in order to predict the solidification curve, independently of the melting, in order to verify the existence of huge hysteresis in large nanoparticles, as the one found in our molecular dynamics simulations.

Acknowledgements

The authors acknowledge the financial support offered by COST-Action MP0903. LP and FB thank the financial support by U.K. research council EPSRC, under Grants No. EP/GO03146/1. The simulations were carried out using the Faculty and Departmental computational facilities at King's College London managed by A. Comisso.

Notes

^a Physics Department, King's College London, WC2R 2LS, U.K.

^b National Research Council (CNR-IENI), Via De Marini 6, 16149-Genoa, Italy

† Footnotes should appear here. These might include comments relevant to but not central to the matter under discussion, limited experimental and spectral data, and crystallographic data.

Electronic Supplementary Information (ESI) available: [details of any supplementary information available should be included here]. See DOI: 10.1039/b000000x/

References

- 1 R. Ferrando, J. Jellinek and R.L. Johnston, *Chem. Rev.*, 2008, **108**, 845.
- 2 F. Baletto and R. Ferrando, *Rev. Mod. Phys.*, 2005, **77**, 371.

- 3 I. Parsina and F. Baletto, *J. Phys. Chem. C.*, 2010, **114**, 1504.
- 4 I. Parsina, C. DiPaola and F. Baletto, *Nanoscale*, 2012, **4**, 1160.
- 5 D. Alloyeau, et al., *Nature Materials*, 2009, **8**, 940.
- 6 C. Langlois, D. Alloyeau, Y. Le Bouar, A. Loiseau, T. Oikawa, C. Mottet and C. Ricolleau, *Faraday Discussion*, 2008, **138**, 375.
- 7 L.-L. Wang, T.L. Tan and D.D. Johnson, *Nano Lett.*, 2014, **14**, 7077.
- 8 G. Guisbiers, S. Khanal, F. Ruiz-Zepeda, J. Roque de la Puente and M. José-Yacamán, *Nanoscale*, 2014, **6**, 14630.
- 9 G. Guisbiers, S. Mejia-Rosales, S. Khanal, F. Ruiz-Zepeda, R.L. Whetten and M. José-Yacamán, *Nano Lett.*, 2014, **14**, 6718.
- 10 G. Guisbiers and G. Abudukelimu, *J. Nanopart. Res.*, 2013, **15**, 1431.
- 11 G. Guisbiers, G. Abudukelimu and D. Hourlier, *Nano Res. Lett.*, 2011, **6**, 396.
- 12 B. Lim, T. Yu and Y. Xia, *Angew. Chemie Int. Ed.*, 2010, **49**, 9819.
- 13 C. di Paola and F. Baletto, *Phys. Chem. Chem. Phys.*, 2011, **13**, 7701.
- 14 T. Takahashi, M. Kawabata, T. Kai, H. Kimura and A. Inoue, *Mater. Trans.*, 2006, **47**, 2081.
- 15 K. Sasaki et al., *Angew. Chem. Int. Ed.*, 2010, **49**, 8602.
- 16 P.C. Jennings et al., *J. Phys. Chem. C*, 2015, DOI: 10.1021/jp511598e.
- 17 P.C. Jennings, H.A. Aleksandrov, K.M. Neyman, R.L. Johnston, *Nanoscale*, 2014, **6**, 1153.
- 18 J. Greeley et al., *Nature Chem.*, 2009, **1**, 552.
- 19 M.A. Asoro, D. Kovar, Y. Shao-Horn, L.F. Allard and P.J Ferreira, *Nanotechnology*, 2010, **21**, 025701.
- 20 S. Khanal et al., *Beilstein J. Nanotechnol.*, 2014, **5**, 1371.
- 21 L. Su et al., *J. Mater. Chem. A*, 2013, **1**, 12293.
- 22 D. Xu et al., *Angew. Chem.*, 2010, **122**, 1304.
- 23 K. Yun et al., *Acta Mater.*, 2012, **60**, 4908.
- 24 P. Strasser et al., *Nat. Chem.*, 2010, **2**, 454.
- 25 M. Wautelet and A.S. Shirinyan, *Pure Appl. Chem.*, 2009, **81**, 1921.
- 26 J.J. Thomson, *Application of Dynamics to Physics and Chemistry*, Mc-Millan, London, 1888.
- 27 P. Pawlow, *Z. Phys. Chem.*, 1909, **65**, 545.
- 28 A. Barybin and V. Shapovalov, *J. Appl. Phys.*, 2011, **109**, 1.
- 29 H. Reiss and I. B. Wilson, *J. Colloid Sci.*, 1948, **3**, 551.
- 30 C.H. Huang, H.P. Wang, J.E. Chang and E.M. Eyring, *Chem. Commun*, 2009, **31**, 4663.
- 31 Z.L. Wang, J.M. Petroski, T.C. Green and M.A. El-Sayed, *J. Phys. Chem. B*, 1998, **102**, 6145.
- 32 N. Saunders and A.P. Miodownik, *CALPHAD (Calculation of Phase Diagrams): A Comprehensive Guide*, Exeter, Pergamon, 1998.
- 33 T. Tanaka and S. Hara, *Z. Metallkd.*, 2001, **92**, 467.

- 34 I .Egry, E. Ricci, R. Novakovic and S. Ozawa, *Adv. Colloid Interface Sci.*, 2010, **159**, 198.
- 35 J. Park and J. Lee, *Comput. Coupling Phase Diagrams Thermochem.*, 2008, **32**, 135.
- 36 G. Garzel, J. Janczak-Rusch and L. Zabdyr, *Comput. Coupling Phase Diagrams Thermochem.*, 2012, **36**, 52.
- 37 W.A. Jesser, R.Z. Shneck and W.W. Gile, *Phys. Rev. B*, 2004, **69**, 144121.
- 38 J. Sopoušek et al., *Comput. Coupling Phase Diagrams Thermochem.*, 2014, **45**, 33.
- 39 J. Sopoušek, J. Vřešťál, A. Zemanova and J. Bursik, *J. Min. Metall. Sect. B-Metall.*, 2012, **48**, 419.
- 40 F. Baletto, C. Mottet and R. Ferrando, *Chem. Phys. Lett.*, 2002, **354**, 82.
- 41 C. Mottet, G. Rossi, F. Baletto and R. Ferrando, *Phys. Rev. Lett.*, 2005, **95**, 035501.
- 42 F. Baletto, C. Mottet and R. Ferrando, *Phys. Rev. Lett.*, 2000, **84**, 5544.
- 43 F. Baletto, R. Ferrando, A. Fortunelli and C. Mottet, *J. Chem. Phys.*, 2002, **116**, 3856.
- 44 G. Guisbiers, G. Abudukelimu, F. Clement and M. Wautelet, *J. Comput. Theor. Nanosci.*, 2007, **4**, 309.
- 45 H.M. Lu, P.Y. Li, Z.H. Cao and X.K. Meng, *J. Phys. Chem. C*, 2009, **113**, 7598.
- 46 T. Abe, B. Sundman and H. Onodera, *J. Phase Equilib.*, 2006, **27**, 5.
- 47 A. Passerone, M.L. Muolo, F. Valenza and R. Novakovic, *Surf. Sci.*, 2009, **603**, 2725.
- 48 T. Ishikawa et al., *Jpn. J. Appl. Phys.*, 2006, **45**, 1719.
- 49 V.K. Kumikov and Kh. B. Khokonov, *J. Appl. Phys.* 1983, **54**, 1346.
- 50 T. Iida and R.I.L. Guthrie, *The physical properties of liquid metals*, Clarendon, Oxford, 1993.
- 51 X.-G. Lu, M. Selleby and B. Sundman, *Comput. Coupling Phase Diagrams Thermochem.*, 2005, **29**, 68.
- 52 M. Wautelet, J.P. Dauchot and M. Hecq, *Nanotechnology*, 2000, **11**, 6.
- 53 A.S. Barnard, X.M. Lin and L.A. Curtiss, *J. Phys. Chem.*, 2005, **109**, 24465.